American Mineralogist, Volume 91, pages 1773–1782, 2006

A XANES study of Cu speciation in high-temperature brines using synthetic fluid inclusions

Andrew J. Berry,[1,*] Alistair C. Hack,[1] John A. Mavrogenes,[1,2] Matthew Newville,[3] and Stephen R. Sutton[3,4]

[1]Research School of Earth Sciences, Australian National University, Canberra, ACT 0200, Australia
[2]Department of Earth and Marine Sciences, Australian National University, Canberra, ACT 0200, Australia
[3]Consortium for Advanced Radiation Sources (CARS), University of Chicago, Chicago, Illinois 60637, U.S.A.
[4]Department of Geophysical Sciences, University of Chicago, Chicago, Illinois 60637, U.S.A.

Abstract

Cu *K*-edge X-ray absorption near edge structure (XANES) spectra were recorded from individual synthetic brine fluid inclusions as a function of temperature up to 500 °C. The inclusions serve as sample cells for high-temperature spectroscopic studies of aqueous Cu-Cl speciation. Cu^+ and Cu^{2+} can both be identified from characteristic pre-edge features. Mixed oxidation states can be deconvoluted using linear combinations of Cu^+ and Cu^{2+} spectra. This work illustrates how complex Cu XANES spectra can be interpreted successfully. Cu^{2+} is the stable oxidation state in solution at room temperature and Cu^+ at high temperatures. The change in oxidation state with temperature was completely reversible. Cu^+ was found to occur exclusively as the linear species $[CuCl_2]^-$ in solutions containing KCl with Cu:Cl ratios up to 1:6. In the absence of K^+, there is evidence for higher order coordination of Cu^+, in particular the tetrahedral complex $[CuCl_4]^{3-}$. The importance of such complexes in natural ore-forming fluids is yet to be determined, but may explain the vapor-phase partitioning of Cu as a Cl complex from a Cl-rich brine.

Keywords: XAS (XAFS, XANES), Cu in high-temperature brines, high-temperature studies, XANES of fluid inclusions, fluid phase, experimental petrology, synthetic fluid inclusions

Introduction

Ore deposits such as porphyry Cu and epithermal Au(Cu) form from metals transported as complex ions in hydrothermal solutions (Barnes 1979). To understand metal solubilities, the partitioning of metals among melt, brine, and vapor, and the mechanism of ore deposition, it is necessary to determine the nature of the metal complexes and their stability as a function of variables such as temperature and fluid composition.

In magmatic hydrothermal fluids Cu occurs as Cu^+, with Cl^- and HS^- being the most abundant potential ligands (e.g., Seward and Barnes 1997). HS^- forms complexes with Cu^+ under reduced, near-neutral to alkaline conditions with high total S concentrations (Shea and Helz 1988; Helz et al. 1993; Thompson and Helz 1994; Mountain and Seward 1999, 2003). The importance of these complexes, however, is probably minor in the high-temperature acidic fluids, containing S as both H_2S and SO_2, which are typically exsolved from volcanic arc magmas (Giggenbach 1987). Under such conditions Cu^+-Cl complexes are likely to be important, and Cu^+ speciation in brines has been investigated by solubility and spectroscopic experiments, mostly at temperatures less than 350 °C (Romberger and Barnes 1970; Crerar and Barnes 1976; Varyash and Rekharsky 1981; Hemley et al. 1992; Varyash 1991; Seyfried and Ding 1993; Xiao et al. 1998; Fulton et al. 2000a; Liu et al. 2001, 2002; Archibald et al. 2002). These studies indicate that $[CuCl]^0$ and $[CuCl_2]^-$ dominate at most Cl concentrations (e.g., Xiao et al. 1998; Liu et al. 2001, 2002). Higher order complexes with the stoichiometry $[CuCl_n]^{1-n}$, where $n > 2$, are considered insignificant for all but the most saline hydrothermal fluids (Liu et al. 2002). The absence of data for near-magmatic temperatures (500–850 °C) limits our understanding of porphyry Cu ore genesis. Whereas depositional conditions are fairly well constrained (Hezarkhani et al. 1999), little is known about the earliest stages of the ore-forming process in which Cu is extracted from the magma during degassing and transported hydrothermally to the site of deposition (Harris et al. 2003).

Fluid modeling based on low-temperature data for aqueous species is commonly used to try and understand high-temperature processes, but the validity of thermodynamic extrapolations into the "supercritical" region (characteristic of many magmatic hydrothermal systems) is questionable (Sverjensky et al. 1997; Akinfiev and Zotov 2001). Furthermore, although generally assumed, it is uncertain whether the species described at low temperatures remain important at magmatic temperatures.

The paucity of solubility and speciation data for high-temperature and high-pressure fluids is largely due to the limitations of traditional experimental techniques. For example, in situ spectroscopic methods usually are restricted to subcritical, vapor-saturated conditions, whereas studies that rely on post-quench chemical analysis of high-temperature solutions can suffer from solute precipitation on cooling and decompression.

* Present Address: Department of Earth Science and Engineering, Imperial College London, South Kensington, SW7 2AZ, U.K. E-mail: a.berry@imperial.ac.uk

0003-004X/06/1112–1773$05.00/DOI: 10.2138/am.2006.1940

These experimental difficulties can be avoided if hydrothermal fluids are trapped as inclusions in a mineral phase. Microanalytical techniques such as laser-ablation inductively coupled plasma mass spectrometry (LA-ICPMS), particle-induced X-ray emission (PIXE), synchrotron X-ray fluorescence (SXRF), and X-ray absorption near-edge structure (XANES) spectroscopy are all suitable for obtaining solubility information from individual inclusions, while XANES has the added advantage of allowing the speciation to be determined. Here we report Cu *K*-edge XANES spectra for Cu-Cl solutions, of varying Cu:Cl ratio and composition, trapped in situ under hydrothermal conditions as synthetic fluid inclusions in quartz. The inclusions can be reheated, allowing their use as sample cells for high-temperature spectroscopic studies of "supercritical" fluids (Anderson et al. 1995; Mavrogenes et al. 2002).

Cu *K*-edge XANES spectroscopy

XANES spectroscopy is an element-specific technique that can provide information on the oxidation state and coordination environment of a metal ion in solution. *K*-edge XANES spectra are recorded by monitoring the absorption of X-rays, associated with the excitation of a *K* shell (1s) electron to higher energy states, as a function of X-ray energy. The onset of these transitions gives rise to the *K* absorption edge. In this work, absorption is detected from the intensity of the Cu$K\alpha$ fluorescence, emitted when an outer-shell electron falls into the *K*-shell vacancy created by the electronic transition. The energy and intensity of the transitions are dependent upon the oxidation state, coordination symmetry, and ligand type, and thus, XANES features can provide detailed chemical information. In general terms, transitions (including the absorption edge) shift to higher energy with increasing oxidation state and gain intensity in low-symmetry environments (Wong et al. 1984; Sutton et al. 1993; Bajt et al. 1994; Berry et al. 2003; Berry and O'Neill 2004; Farges 2005).

Copper *K*-edge XANES spectra of both Cu^{2+} and Cu^{+} contain features that are diagnostic of the oxidation state and speciation. Example XANES spectra for Cu^0, Cu^+, and Cu^{2+} are given in Figure 1a. These show the expected shift of the absorption edge to higher energy with increasing oxidation state and differences in the edge shape. The edge shift between Cu^+ and Cu^{2+} is typically large (>5 eV) and derives from an intense Cu^+ pre-edge feature (1s $\rightarrow$ 4p) that merges with, and is usually referred to as, the absorption edge (Fulton et al. 2000b). Features comprising the edge are often more easily identified in the derivative spectra [d(intensity)/d(energy)], shown in Figure 1b, in which inflections appear as peaks.

Cu^{2+} has a d^9 electronic configuration resulting in either a static or dynamic Jahn-Teller distortion of the coordination to remove the electronic degeneracy. This manifests itself as an elongation of the axial ligands (defined here as the z direction) away from an octahedral geometry toward tetragonal coordination. This axial or tetragonal distortion is characterized by a shoulder on the main absorption edge (Fig. 1a), with the energy separation of this shoulder from the edge being related to the degree of distortion from octahedral. This energy difference allows a quantitative measure of axial bond lengths with the predicted distortion of Cu^{2+}-Cl complexes in aqueous solutions being ~0.6 Å (Onori et al. 1988; Garcia et al. 1989). The shoulder also decreases in energy with increasing covalency of the equatorial ligands (Kau et al. 1987). This feature cannot be resolved for distortions less than ~0.3–0.4 Å, in which case it is most easily seen as a splitting of the corresponding peak in the derivative spectrum. These split components have been referred to as α and β peaks (Fig. 1b), where α corresponds to the shoulder and β to the main absorption edge (Palladino et al. 1993; Alcacio et al. 2001).

The Cu^{2+} absorption-edge shoulder, which is strongly z polarized, has been assigned to several processes including a "shakedown" involving a Cu^{2+} 1s $\rightarrow$ 4p transition simultaneous with ligand-to-metal charge transfer [final state $(1s)^1(3d)^{10}4p^1\underline{L}$, where $\underline{L}$ is a ligand hole] (Bair and Goddard 1980; Kau et al. 1987), a 1s $\rightarrow$ $4p_z$ bound-to-bound state transition (Smith et al. 1985), and to multiple scattering from the axial ligands (Onori et al. 1988). The absorption crest has been also attributed to the 1s $\rightarrow$ 4p transition (Bair and Goddard 1980) as well as to transitions to continuum states (Smith et al. 1985).

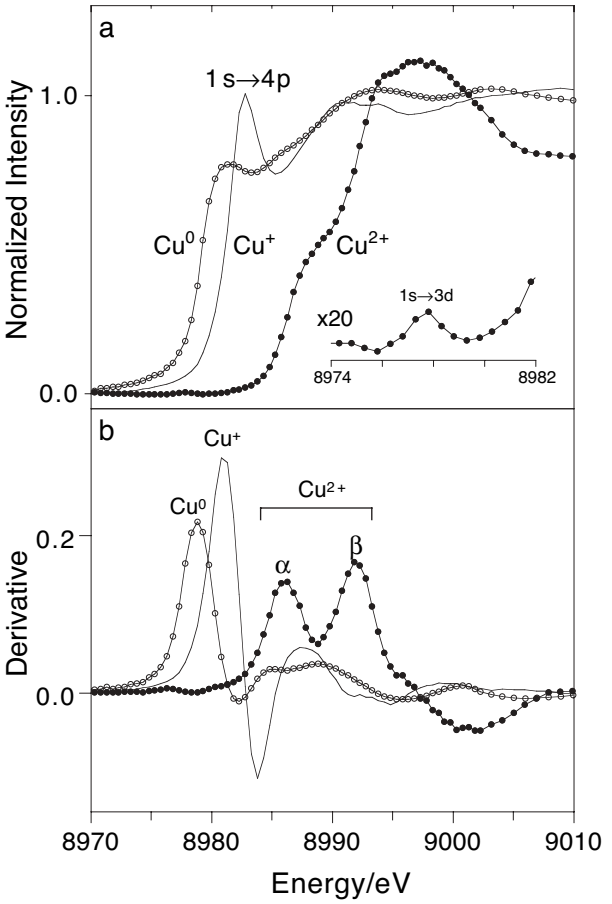

Figure 1. Representative Cu *K*-edge (**a**) XANES and (**b**) derivative spectra for Cu^0 (metal), Cu^+ (AH87 at 400 °C), and Cu^{2+} (AH88 at 25 °C). Cu^+ is characterized by a 1s $\rightarrow$ 4p transition at ~8983 eV. A shoulder on the Cu^{2+} absorption edge indicates a tetragonal distortion of octahedral coordination and results in the two derivative peaks labeled α (shoulder) and β (crest). Cu^{2+} is also characterized by a weak 1s $\rightarrow$ 3d transition at ~8978 eV (inset) that cannot occur for the closed-shell d^{10} configurations of Cu^0 and Cu^+.

The speciation of Cu^{2+} in NaCl solutions varies with Cl^- concentration and temperature (D'Angelo et al. 1997; Collings et al. 2000), although in general terms, Cl^- appears to replace an axial O in $Cu(H_2O)_6^{2+}$ at low Cl^- concentrations, and occupies both axial and equatorial positions at higher concentrations. The change in Cu^{2+} coordination with increasing Cl^- content is also evidenced by changes in the color of solutions from blue to green (D'Angelo et al. 1997; Collings et al. 2000). The tetragonal distortion produced by Cu:Cl ratios ranging from 1:2 to 1:30 does not produce a pronounced shoulder and only a small splitting is observed in the derivative spectrum (D'Angelo et al. 1997). Pronounced shoulders are, however, observed for Cu^{2+} in OH^- solution (Onori et al. 1988) and solid CuO (Garcia et al. 1989).

The spectra of Cu^{2+} complexes also exhibit a characteristic weak feature around 8978 eV attributed to the 1s → 3d transition (Kau et al. 1987; Fulton et al. 2000a, 2000b). This feature is diagnostic of Cu^{2+} as the transition cannot occur for the closed shell d^{10} configuration of Cu^+.

In an extensive XANES study of 59 reference compounds (40 Cu^{2+} and 19 Cu^+), Kau et al. (1987) found that no Cu^{2+} complex exhibits a significant peak below 8985 eV and that a peak between 8983 and 8984 eV is diagnostic of Cu^+. This sharp pre-edge feature (at 8983 eV in Fig. 1a) has been assigned to the Cu^+ 1s → 4p transition (Kau et al 1987; Blackburn et al. 1989). The intensity of the transition is dependent on the coordination environment; it is most intense for Cu^+ in linear coordination, for which it has a normalized absorption of 1.08 ± 0.10, whereas three- and four-coordinated complexes have normalized peak heights of 0.63 ± 0.05 and 0.72 ± 0.06, respectively (Kau et al. 1987). In linear coordination, the transition is to a pure metal p final state, which is strongly Laporte allowed. For higher coordinations, mixing of 4s character (to which transitions from 1s are forbidden) into the p state decreases the allowedness and hence intensity of the transition (Blackburn et al. 1989). The transition may also shift in energy with coordination number (Blackburn et al. 1989; Kau et al. 1987). These results were used to determine quantitatively the Cu oxidation state and the Cu^+ coordination geometry in proteins (Kau et al. 1987; Blackburn et al. 1989), and to identify the oxidation state and structure of Cu in hydrothermal solutions (Fulton et al. 2000a, 2000b).

Studies of Cu-X (where X = Cl^- or Br^-) solutions at temperatures up to 325 °C found, from the presence and intensity of the pre-edge feature at 8983 eV and EXAFS models, that $[CuX_2]^-$ is the only stable Cu complex above 100 °C for X^- concentrations up to 2.0 *M*, corresponding to a Cu:X ratio of 1:4 (Fulton et al. 2000a, 2000b). No evidence was found for higher order complexes, i.e., $[CuX_3]^{2-}$ or $[CuX_4]^{3-}$. For Cu:X ratios <2 the linear geometry was maintained by the formation of $CuX(H_2O)$. Similar linear complexes were also observed by Mavrogenes et al. (2002) above 200 °C for Cu in natural low-density vapor inclusions from the Mole Granite.

Experimental methods

Samples of mineral-buffered hydrothermal fluid were trapped as synthetic fluid inclusions in pre-fractured quartz using Cu^0 capsules and a piston-cylinder apparatus (Sterner and Bodnar 1984; Brodholt and Wood 1994; Loucks and Mavrogenes 1999). The fluid redox potential and pH were buffered by either Cu + cuprite + talc + quartz (Cu + Cpr + Tc + Qz; Cl added as $CuCl_2$), or Cu + magnetite + hematite + orthoclase + quartz + sillimanite (Cu + Mt + Hm + Kf + Qz + Sil; Cl added as KCl). The Cu content of individual inclusions was determined by LA-ICPMS (Günther et al. 1998; Loucks and Mavrogenes 1999) and PIXE (Heinrich et al. 1992). Samples were prepared at temperatures and pressures given in Table 1. These experiments are part of a series of Cu solubility experiments that will be reported in detail elsewhere (Hack and Mavrogenes 2006).

Inclusions chosen for study were typically well-formed and equant and ranged in size from 20 to 50 μm. XANES spectra were recorded at beamline 13-ID-C, GeoSoilEnviroCARS (GSECARS), of the Advanced Photon Source, Argonne National Laboratory, U.S.A. The polished quartz sections hosting the inclusions were held in a windowless Linkam TS1500 heating stage mounted vertically at 45° to both the X-ray beam and detector. The inclusion temperature was estimated from thermocouple measurements at the top and bottom surfaces of the sample and is within ±10 °C of the quoted value. Homogenization temperatures were determined ex situ provided an internal reference for the sample temperature.

The excitation energy of the incident X-ray beam was selected using a Si(111) double crystal monochromator. The energy was calibrated by defining the first derivative peak in the spectrum of Cu foil as 8978.9 eV; the expected monochromator reproducibility over the duration of the beamtime is ~0.1 eV. To maintain the peak X-ray intensity from the undulator, the undulator gap was moved simultaneously with the monochromator energy. Beam intensity stability was maintained by detuning the monochromator to ~50% of the maximum X-ray intensity and using closed-loop feedback (ion chamber signal source) on the second crystal angle. The beam was focused using Kirkpatrick-Baez (KB) mirrors (Eng et al. 1998) to a spot size of 5–10 μm. The critical angle cut-offs of the mirrors provide excellent rejection of high-energy harmonics. The beam size and location were determined using a Ce-doped YAG phosphor viewed with a long-working-distance objective and CCD camera, allowing the beam to be positioned accurately not only on individual inclusion, but also on selected regions of an inclusion. In this way, daughter crystals or shrinkage bubbles could be avoided (or analyzeds) and solution spectra acquired at all temperatures. A shield was used to block stray radiation, but allow full illumination of a 16 element Ge array detector, from which the integrated intensity of the Cu*K*α fluorescence line was selected and recorded digitally. XANES spectra were acquired by scanning the energy from 8970 to at least 9075 eV with a step size of 0.5 eV over the absorption edge, with count times of 1 s per point. Typical scan times were around 3 to 4 min. Inclusions were viewed while spectra were recorded allowing any change in the area being analyzed (e.g., movement of the shrinkage bubble) to be noted. Spectra were recorded at variable temperatures up to and beyond the homogenization of the inclusion. The maximum temperature was limited by inclusion decrepitation. For each condition, several spectra were recorded sequentially to observe any changes with time indicative of beam damage. Spectra were compared after subtraction of a linear baseline and normalization to the average absorption coefficient above 9050 eV.

Results

A typical fluid inclusion is shown in Figure 2. At room temperature the inclusion contains condensed liquid, a vapor-shrinkage bubble, and a colorless to brown tetrahedral daughter crystal. The morphology of the crystal, its absence in similar Cl-free experiments, and a correlation between crystal size and Cl concentration (related to Cu solubility) are consistent with the cubic mineral nantokite (CuCl). The crystal appears to be unstable at room temperature and rapidly decomposes with exposure to laser (Raman), particle (PIXE), and X-ray beams. For each sample the phase proportions are uniform and all inclusions completely homogenize at a constant temperature. Sample AH87 also contains crystals of sylvite (KCl) at room temperature. The homogenization temperatures (T_h), Cu concentrations, and Cu:Cl ratios are given in Table 1.

XANES spectra are best interpreted with reference to a series of standards in which the oxidation state and coordination environment are well understood. Although we do not report standard spectra ourselves, we have based our spectral interpretation on the work of Kau et al. (1987), which presented results for 40 Cu^{2+} and 19 Cu^+ reference compounds. In particular, a peak between 8983 and 8984 eV is diagnostic of Cu^+ ("an immediate and definitive indication of the oxidation state;" Fulton et al.

TABLE 1. Experimental conditions, fluid compositions, and dominant complexes at T_h

Sample	Buffer	*T* (°C)	*P* (MPa)	T_h (°C)	Cu (wt%)	Cl (wt%)	K (wt%)	Cu_{mol}:Cl_{mol}	Complex
AH88	Cu+Mt+Hm+Kf+Sil+Qz	700(25)	341(5)	375(3)	10.4(5.7)	14.6	7.4	1:2.5	$[CuCl_2]^-$
AH87	Cu+Mt+Hm+Kf+Sil+Qz	700(25)	313(5)	380(3)	8.5(4.0)	29.3	20.6	1:6.3	$[CuCl_2]^-$
R177	Cu+Cpr+Tc+Qz	630(5)	338(6)	–	15.2(8.9)	24.2	0	1:2.9	$[CuCl_{3/4}]^{2-/3-}$

Note: The Cl content is that expected from the amount of either KCl or $CuCl_2$ added to the capsule (Hack and Mavrogenes 2006).

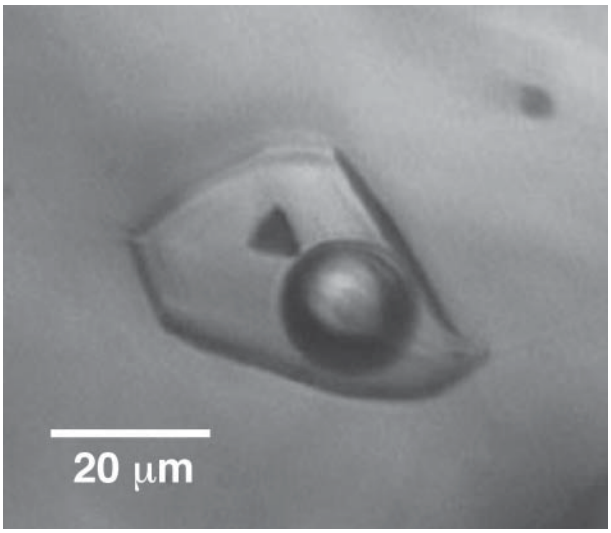

FIGURE 2. Optical image of a typical fluid inclusion (sample AH88) at room temperature comprising fluid, a shrinkage bubble, and crystal of nantokite (CuCl).

2000b, p. 11,654) as no major Cu^{2+} peaks occur below 8985 eV. Furthermore, the intensity of this peak is a strong indicator of the coordination symmetry. Cu^{2+}, on the other hand, is characterized by a weak feature at ~8978 eV. Cu^{2+} coordinated to O also results in a broad peak at ~8995–9000 eV (Fulton et al. 2000a). The results of the present and earlier studies can be compared with confidence, because in all cases, the energy is calibrated with respect to Cu foil and the spectral resolution is similar, as indicated by the smaller maximum intensities of the 8983 eV peak (linear coordination) in Kau et al. (1987), Fulton et al. (2000a), and this work.

Although transitions characteristic of Cu^+ and Cu^{2+} occur at sufficiently different energies so as not to overlap, the analysis of XANES spectra still can be difficult because the shape of an absorption edge may vary due to contributions from multiple oxidation states or, for a given oxidation state, differences in the intensity of transitions comprising the edge (dependent on coordination). The presence of Cu^0 can be readily identified by the low-energy onset of the absorption edge and the resulting "calibration peak" in the derivative spectrum. In the absence of significant Cu^0, the 1s → 4p transition of Cu^+ is the next lowest energy feature producing diagnostic intensity at ~8983 eV and a derivative peak at approximately constant energy (8981 eV). Cu^{2+} on its own is characterized by an edge shoulder and the resulting α and β peaks in the derivative spectrum. These derivative features, however, are not observed for the spectral profile that results when Cu^{2+} coexists with significant Cu^+. A Cu^{2+} contribution to a spectrum unambiguously containing Cu^+ can be identified either from the presence of the weak 1s → 3d feature ~8978 eV or by successful modeling of the spectrum as a linear combination of the expected "end-member" Cu^+ and Cu^{2+} spectral components. On this basis, it is thus possible to deconvolute and interpret complex Cu XANES spectra.

A significant problem associated with the analysis of fluids using high-flux X-rays is the possibility of beam-induced chemical changes (Jayanetti et al. 2001). In some cases, this was observed visibly by decomposition of the nantokite crystal, a darkening of the fluid color, or the appearance of an immiscible phase within the shrinkage bubble. It was necessary to attenuate the photon flux (by detuning the monochromator) by varying amounts (depending upon fluid composition and temperature) to avoid beam damage; most spectra were acquired using a flux of ~10^{10} photons/s. All spectra were recorded repeatedly as a function of time so that changes associated with beam exposure could be readily identified. Two examples of beam damage are shown in Figure 3. The top series of spectra illustrate the decomposition of Cu^+ in solution to Cu^0 (similar to as reported by Jayanetti et al. 2001), which precipitates on the walls of the inclusion. The precipitation increases with beam exposure time resulting in accumulation of Cu^0 in the part of the inclusion analyzed by the beam and a systematic increase in the fluorescence intensity. This is accompanied by a progressive change in the edge shape (seen clearly in the derivative spectra). The bottom series of spectra show an initial oxidation of Cu^+ to Cu^{2+} followed by reduction to Cu^0. The oxidation states contributing to the spectra are identified clearly in the derivative. Although beam damage can occur extremely quickly (in a matter of seconds) and rapid beam induced changes cannot be discounted, the time scale of the spectral acquisition does allow systematic changes in the (expected) spectra with beam exposure to be identified, monitored, and avoided.

AH88

Cu *K*-edge XANES spectra for sample AH88 are shown in Figure 4. Spectra recorded at room temperature (25 °C in Fig. 4a) are characteristic of Cu^{2+} (α and β peaks in the derivative spectrum and 1s → 3d pre-edge feature; also see Fig. 1). At higher temperatures the spectrum recorded at 360 °C (Fig. 4a) was obtained. This spectrum is typical of that acquired from ten different inclusions at temperatures from 185 to 485 °C. Spectra recorded sequentially as a function of time (up to ~10) were identical. The peak in the XANES spectrum at 8983 eV corresponds to the 1s → 4p transition of Cu^+. The normalized intensity of this feature (~1.08) is consistent with linear coordination (Kau et al. 1987). The spectrum is also indistinguishable from those reported by Fulton et al. (2000a) and Mavrogenes et al. (2002) and assigned to $[CuCl_2]^-$. There is some variability in the intensity of the 8983 eV peak between ~0.91 and 1.08 (e.g., 1.00 in the spectrum recorded at 260 °C), although there is no trend with temperature.

The change in oxidation state from Cu^{2+} to Cu^+ with increasing temperature is fully reversible, as shown in Figure 4 by

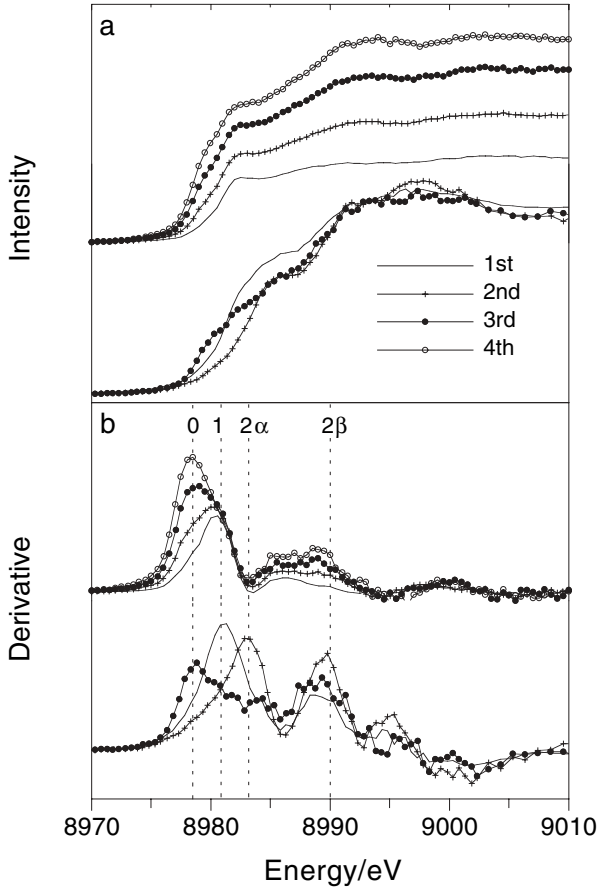

FIGURE 3. Cu *K*-edge (**a**) XANES and (**b**) derivative spectra illustrating the effects of beam damage. Spectra are shown for two different samples; the order in which the spectra were acquired is indicated. The top series illustrates the precipitation of Cu^0 from Cu^+ in solution. The bottom series shows $Cu^+ \rightarrow Cu^{2+} \rightarrow Cu^0$. The oxidation states associated with the derivative peaks are indicated by the dashed lines.

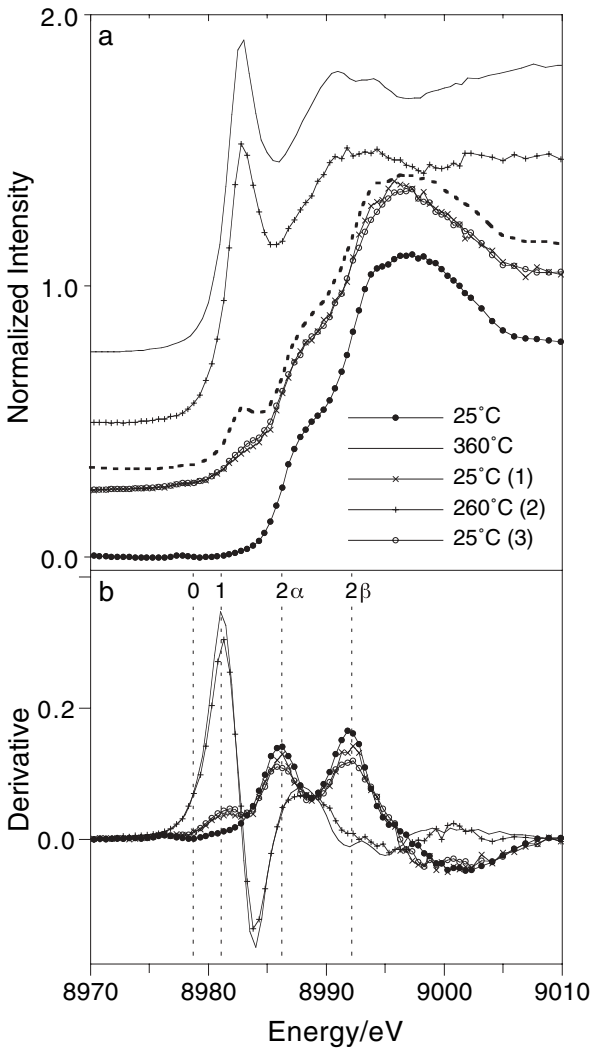

FIGURE 4. Cu *K*-edge (**a**) XANES and (**b**) derivative spectra of fluid inclusions from AH88. Spectra are offset for clarity. The top spectrum in **a** (recorded at 360 °C) corresponds to $[CuCl_2]^-$ and is typical of spectra recorded for this sample above ~200 °C. Three of the spectra in **a** were recorded in the order indicated in parentheses and illustrate the reversibility of the change in oxidation state between Cu^{2+} and Cu^+ with temperature. The other 25 °C spectrum was recorded from a different inclusion. The dashed spectrum corresponds to a linear combination of the 360 (20%) and 25 °C (80%) spectra. The oxidation states associated with the derivative peaks are indicated by the dashed lines in **b**.

the series of spectra recorded at 25 °C (1), 260 °C (2), and 25 °C (3), where the numbers in parentheses indicate the order in which the spectra were acquired. The 25 °C spectra correspond to Cu^{2+} coexisting with a small amount of Cu^+. Interestingly, it is not possible to reproduce these mixed oxidation state spectra from a linear combination of the Cu^{2+} (25 °C) and Cu^+ (360 °C) spectra. The best fit, shown in Figure 4a, overestimates the intensity of the 1s → 4p component. The fit would be improved if the intensity of this transition were reduced, as expected if Cu was coordinated to three or four ligands.

Cu^+ at room temperature is metastable and rapidly converts to Cu^{2+} (usually within a single spectral scan). Similar behavior was observed at 120 °C, although the rate of reaction was slower, while at 185 °C Cu^+ appears stable. The conversion of Cu^+ to Cu^{2+} with beam exposure at room temperature is consistent with a darkening of many inclusions since Cu^{2+}, unlike Cu^+, absorbs visible light. This dark color disappears on heating.

AH87

Spectra for five different inclusions of AH87 at ~400 °C are shown in Figure 5. The spectrum for the inclusion numbered 1 is essentially identical to that observed for AH88, corresponds to $[CuCl_2]^-$, and was obtained over the entire high-temperature range investigated (325–450 °C). This was the most common spectrum recorded at high temperatures. Cu^{2+} was observed at room temperature with the change from Cu^+ to Cu^{2+} being reversible.

The 400 °C spectrum for inclusion 5 is characteristic of Cu^{2+} (1s → 3d pre-edge feature) with a large tetragonal distortion (large α-β splitting in the derivative spectrum). Spectra for inclusions 2, 3, and 4 represent a progression between the spectra of inclusions 1 and 5. Indeed, these intermediate spectra can be convincingly reproduced by linear combinations of spectra

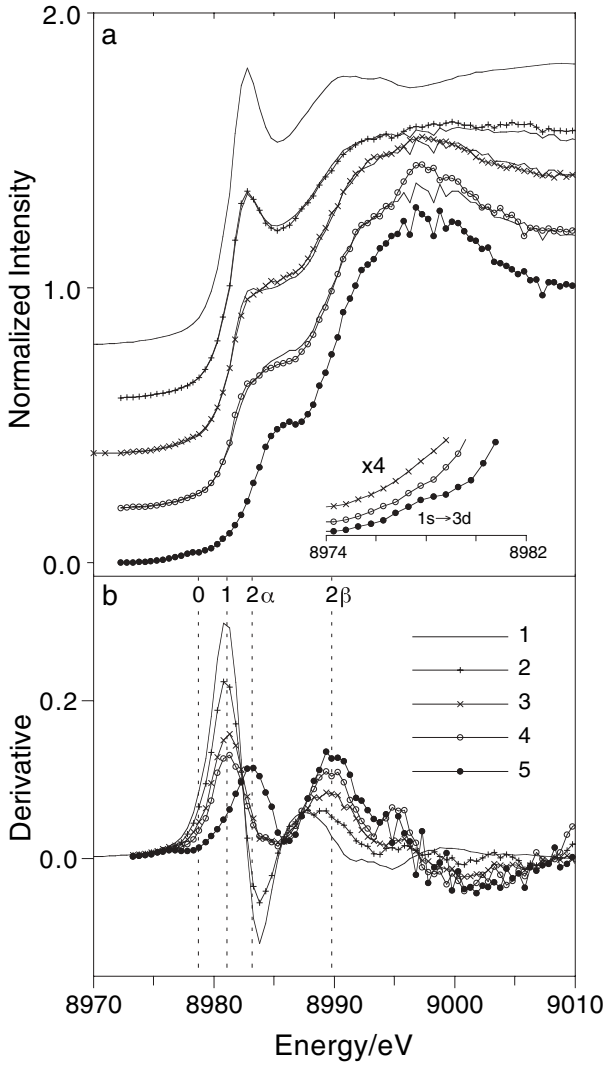

FIGURE 5. Cu *K*-edge (**a**) XANES and (**b**) derivative spectra of solutions trapped in five different fluid inclusions from AH87 at ~400 °C. The spectra for inclusions 1 and 5 correspond to $[CuCl_2]^-$ and Cu^{2+}. The spectra for inclusions 2, 3, and 4 represent a progression between spectra 1 and 5 and can be reproduced using linear combinations of these two end-members (73, 47, and 28% of spectrum 1, respectively). These are shown as the solid lines superimposed on the spectral data. The inset is an expansion of the region containing the 1s → 3d transition characteristic of Cu^{2+}. The oxidation states associated with the derivative peaks are indicated by the dashed lines in **b**.

1 and 5 (73, 47, and 28% of spectrum 1 to reproduce spectra 2, 3, and 4, respectively). The spectra thus represent a mixture of $[Cu^+Cl_2]^-$ and Cu^{2+}, rather than Cu^+ in three- or fourfold-coordination, which could also explain the observed decrease in the 1s → 4p transition intensity. The modeled or fit spectra are superimposed on the raw data in Figure 5. Despite the presence of significant amounts of Cu^{2+} in the intermediate spectra, the 1s → 3d transition could not be identified clearly due to the low signal to noise ratio. Solutions of AH87 appear more susceptible to beam damage than those of AH88.

R177

XANES spectra for inclusions of R177 are shown in Figure 6. For one inclusion a reproducible spectrum of the tetrahedral daughter crystal was obtained at room temperature by greatly reducing the beam intensity (1% of maximum). This spectrum (Fig. 6; CuCl), as expected, corresponds to that reported for solid CuCl (Hamza et al. 1990). In a detailed study of this (elongate) inclusion, the crystal "hot spot" (area of high Cu fluorescence intensity) remained localized at 300 °C producing a $CuCl_{(s)}$-like spectrum. The spectrum from the other end of the inclusion, which contained only solution (Fig. 6; 300 °C), shows a complex edge structure. It is emphasized that the spectrum was constant as a function of time. This spectrum can be approximately modeled as a linear combination of the $CuCl_{(s)}$ (50%) and Cu^{2+} (50%) spectra shown (fit superimposed on spectrum). It cannot be reproduced using $[CuCl_2]^-$ as the Cu^+ component (model using 60% $[CuCl]_2^-$ shown as the dashed spectrum in Fig. 6). Significantly, the spectrum plus that for another inclusion at 400 °C (Fig. 6; 400 °C) shows a weak feature, indicated by the arrow, corresponding to the maximum intensity in $CuCl_{(s)}$. The presence of this feature thus may indicate a $CuCl_{(s)}$-like complex in solution. This feature is not apparent in spectra recorded at 420 and 510 °C; however, these spectra also can be approximately reproduced by linear combinations of the $CuCl_{(s)}$ and Cu^{2+} spectra [shown for the 510 °C spectrum using 25% $CuCl_{(s)}$]. The derivatives of all the high-temperature spectra indicate the presence of Cu^+. The intensity of the Cu^+ 1s → 4p transition in the spectra, or that required to model the spectra in conjunction with a Cu^{2+} component, is reduced significantly from that observed for $[CuCl_2]^-$. This reduction in intensity suggests the presence of higher-order complexes of Cu^+ such as $[CuCl_4]^{3-}$.

The solutions appear more susceptible to beam damage, particularly at elevated temperatures where Cu^0 is produced, than those of AH88 and AH87.

The dominant complex identified at, or near, T_h for each sample is summarized in Table 1.

DISCUSSION

As a general rule, Cu^{2+} was observed in solutions at room temperature and Cu^+ near the homogenization temperature of the inclusions. This behavior is consistent with the temperature dependence of the oxidation state noted by Fulton et al. (2000a, 2000b).

There is some variability in the magnitude of the shoulder on the Cu^{2+} absorption edge (the α-β splitting in the derivative spectrum). A poorly resolved shoulder and small α-β splitting (~4 eV) is typical for $[Cu(H_2O)_6]^{2+}$ and dilute Cu^{2+} in Cl^- solutions with Cu:Cl up to 1:30 (Garcia et al. 1989; D'Angelo et al. 1997; Fulton et al. 2000a). The spectra reported here, for example the room-temperature spectrum of AH88, all exhibit pronounced absorption edge shoulders. The resulting larger α-β splittings (6 eV), which indicate a large tetragonal distortion from octahedral symmetry, are similar to those seen for $CuO_{(s)}$ (Garcia et al. 1989) and Cu^{2+} in NaOH solution (Onori et al. 1988). $CuO_{(s)}$ would seem unlikely in these inclusions since the amount of a solid phase precipitated by beam-induced decomposition should increase with time resulting in an increase in the total fluorescence intensity, which was not observed. The

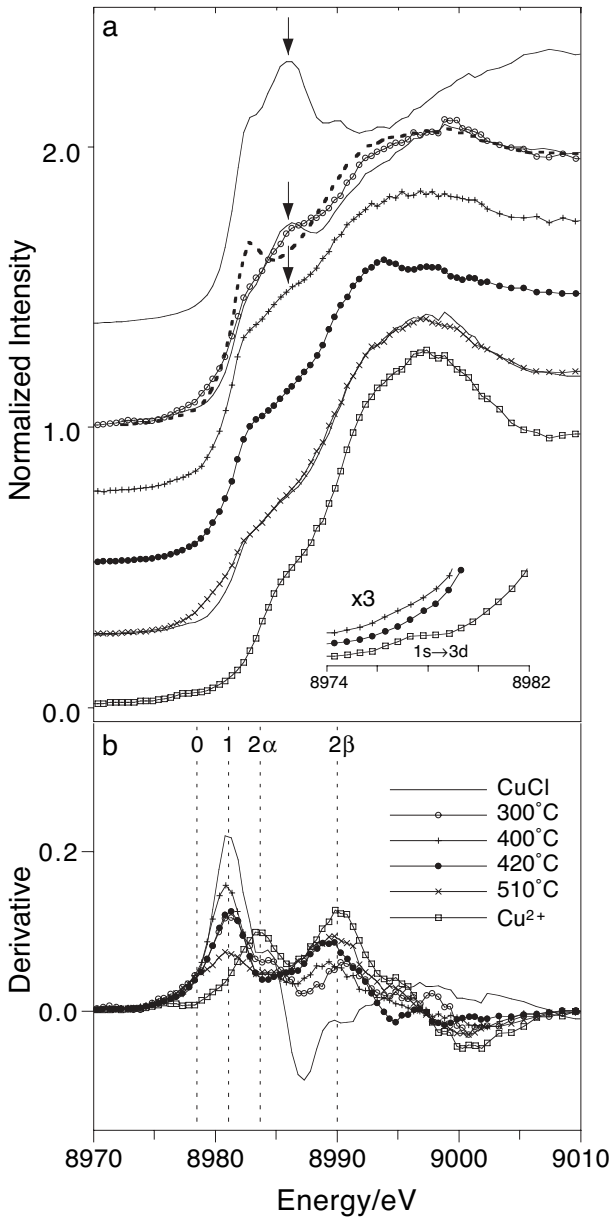

FIGURE 6. Cu *K*-edge (**a**) XANES and (**b**) derivative spectra of fluid inclusions from R177. The spectrum labeled CuCl corresponds to the tetrahedral daughter crystal at 25 °C. The 300 °C spectrum is for the solution of the same inclusion and Cu^{2+} is for a different inclusion at room temperature. The remaining spectra represent a temperature series from a single inclusion. All the high-temperature results can be simulated using linear combinations of the CuCl and Cu^{2+} spectra. These are shown as the solid lines superimposed on selected spectra (300 and 510 °C). The spectra cannot be reproduced using the $[CuCl_2]^-$ spectrum in Figure 5 as the Cu^+ component (dashed spectrum). The arrow indicates the crest in the spectrum of $CuCl_{(s)}$ which is observed in the 300 and 400 °C spectra. The inset shows selected spectra in the region containing the 1s → 3d transition characteristic of Cu^{2+}. The oxidation states associated with the derivative peaks are indicated by the dashed lines in **b**.

presence of a solid is also inconsistent with the rapid reversible reduction to aqueous Cu^+ with increasing temperature (Fig. 4). Thus, we believe that these spectra also correspond to aqueous species. Cu^{2+} coordinated to OH^- is unlikely due to the low pH of the fluids imposed by the buffering mineral assemblage. This large Jahn-Teller distortion may arise from strong coordination of Cl^- to Cu^{2+} in highly concentrated salt solutions where Cl:H_2O is orders of magnitude greater than in the previous studies on dilute systems.

The linear species $[CuCl_2]^-$ is the only Cu^+ complex observed in samples AH88 and AH87. It was found at all temperatures above that at which Cu^{2+} occurs (from ~100 to at least 400 °C). In AH88 it was observed in every inclusion (around ten) and temperature (185 to 485 °C) investigated. In AH87 the $[CuCl_2]^-$ spectrum was that most commonly observed at high temperatures. Other spectra (shown in Fig. 5) can all be reproduced using linear combinations of the spectra for $[CuCl_2]^-$ and Cu^{2+}. $[CuCl_2]^-$ is the expected complex from previous spectroscopic and thermodynamic studies (e.g., Fulton et al. 2000a).

The reversible reduction of Cu^{2+} to Cu^+ with increasing temperature must be associated with the concurrent oxidation of another species. The options for the reductant are limited in these simple systems containing only $Cu^{0/+/2+}$, K^+, H^+, H_2O, and Cl^-. A likely redox reaction is $2Cu^+ + 2H^+ \rightarrow 2Cu^{2+} + H_2$ (as proposed in Mavrogenes et al. 2002). There is circumstantial evidence for the production of a gas phase on cooling; in cases where Cu^+ metastably persists at room temperature, beam exposure results in rapid conversion to Cu^{2+} (change in optical density of the inclusion) and an increase in the size of the shrinkage bubble. In some cases a "second" vapor phase seemed to be produced although this could simply result from an optical alignment of two different bubbles. Although H_2 is highly mobile it would only occur at low temperatures where the rate of diffusion is low (Mavrogenes and Bodnar 1994).

The spectra of AH87 are anomalous both because of the presence of Cu^{2+} at high temperatures (Fig. 5, label 5) and the variable amount that coexists with $[CuCl_2]^-$. We do not believe that this variability represents heterogeneous fluid trapping, but rather post-entrapment oxidation associated with loss of H_2, to different extents, from the inclusions. Clearly if H_2 produced on cooling is subsequently lost from the inclusion, then, in the absence of a suitable reductant, Cu^{2+} will persist at high temperatures. It is not clear why H_2 loss should occur for this sample and not AH88, which was prepared under similar chemical and physical conditions. The important point is that the various spectra can be understood and the contributing species identified.

It is clear from the derivatives of all the high-temperature R177 spectra that Cu^+ contributes to the absorption edge (Fig. 6b). Unambiguous evidence for a Cu^{2+} contribution is less clear due to the low intensity of the 1s → 3d transition, which is obvious only in the Cu^{2+} spectrum (see inset in Fig. 6). The high-temperature spectra can, however, be approximately reproduced by linear combinations of the $CuCl_{(s)}$ and Cu^{2+} spectra. The 400, 420, and 510 °C spectra were recorded from a single inclusion and indicate an increase in the Cu^{2+} component with increasing temperature. At this time, data are not available to determine whether this trend is reversible and hence a characteristic of the solution, or an artifact resulting from increased H_2 loss and as-

sociated oxidation at high temperatures. It is significant, however, that these mixed oxidation state spectra cannot be modeled using $[CuCl_2]^-$ as the Cu^+ component. All such models require a peak around 8983 eV (dashed line in Fig. 6), which is not observed. The model would be improved if the intensity of the 1s → 4p transition at 8983 eV in the Cu^+ component was significantly reduced, as occurs for three- or four-coordinated complexes (Kau et al. 1987). Furthermore, the 300 and 400 °C spectra exhibit a feature, indicated by the arrow in Figure 6, that corresponds to the maximum intensity in the spectrum of $CuCl_{(s)}$. All the spectra can also be reasonably reproduced using $CuCl_{(s)}$ as the Cu^+ end-member. Cu^+ is tetrahedrally coordinated in nantokite and the need for a nantokite component to reproduce the high-temperature spectra suggests that Cu^+ may also be tetrahedrally coordinated in solution. Due to the dependence of Cu solubility on Cl concentration the coordinating ligands are expected to be Cl^- (although H_2O cannot be excluded). Although not conclusive, these spectra provide circumstantial evidence for a complex such as $[CuCl_4]^{3-}$, or so-called higher order coordination of Cu^+. Such highly charged species have been considered unlikely in "supercritical" fluids due to the decrease in the dielectric constant of water with increasing temperature at constant pressure (Seward and Barnes 1997), and thus the actual complex may be $H_3[CuCl_4]$, as suggested by solubility experiments (Hack and Mavrogenes 2006).

Further evidence for higher-order coordination is provided by AH88. The model of the room-temperature spectrum (dashed line in Fig. 4), using $[CuCl_2]^-$ as the Cu^+ component (20%), reproduces the edge well except in the region of the 1s → 4p transition. Once again, the model would be improved if this transition were of lower intensity, as occurs for Cu^+ in higher order coordination. Even though the bulk Cu:Cl ratio in AH88 is ~1:2, the precipitation of $CuCl_{(s)}$ on cooling must result, by stoichiometry, in an increase in the amount of Cl relative to Cu in the liquid phase and a Cu:Cl ratio appropriate for higher-order coordination.

It is expected that higher-order coordination of Cu^+ by Cl^- would be favored by a large molar excess of Cl^-. For the Cu:Cl ratios in AH88 and AH87 (~1:2–1:6) $[CuCl_2]^-$ was the only Cu^+complex identified. Evidence for higher-order complexes was found for R177, which has a Cu:Cl ratio within the range of the other samples (~1:3). The main difference in fluid composition between these samples (given broadly similar pH and redox buffering conditions) is the absence of K in R177. K^+ is an additional cation that competes with Cu^+ for Cl^-; the only other available cation is H^+. The concentrations of Cu^+, K^+, and Cl^- (Table 1) indicate that $[CuCl_2]^-$ is reasonable for AH88 and AH87, but suggest $[CuCl_3]^{2-}$ for R177 (assuming H^+ is relatively minor).

The higher-order complexes of Cu^+ appear unstable relative to $[CuCl_2]^-$. Solutions containing $[CuCl_2]^-$ seem quite stable with respect to beam intensity, exposure time, and temperature. Decomposition, when it does occur, results in the production of Cu^0. In comparison, the higher-order Cu^+ spectra are prone to change rapidly to those typical of either Cu^0 or Cu^{2+}, with both species sometimes being produced in different inclusions of the same sample. This decomposition can occur despite reduction in the beam intensity to levels that are as low as are compatible with the acquisition of a spectrum having adequate signal to noise. In some cases, replicate spectra could be recorded while in others the Cu^+ complex was observed only in the first spectrum with subsequent spectra showing clear evidence of decomposition. The non-reversible change in the Cu oxidation state results from the production of reactive species by the beam (Jayanetti et al. 2001). This is different to the reversible, temperature dependent, redox reaction between Cu^{2+} and Cu^+, and the beam induced conversion of metastable Cu^+ to Cu^{2+} at room temperature.

This work provides circumstantial evidence for higher-order complexes of Cu^+ in high-temperature brines. The coordination of Cu at these conditions has not been studied previously due to the difficulty of acquiring spectroscopic data. From the results of earlier studies and this work, $[CuCl_2]^-$ appears to be the stable complex of Cu^+ in high-temperature fluids over a wide range of temperatures and chloride concentrations. However, in the absence, or low relative abundance, of other cations that compete with Cu^+ for Cl^- (such as Na^+), higher-order complexes, in particular $[CuCl_4]^{3-}$, may be important. The significance of such complexes in systems where Cl >> Cu is yet to be determined and future work will investigate Cu speciation in natural brine inclusions. The extrapolation of low-temperature thermodynamic data for known Cu complexes (i.e., $[CuCl]^0$ and $[CuCl_2]^-$) to describe Cu speciation at magmatic temperatures is clearly inappropriate if additional complexes are present.

The species determined in this study are not necessarily those that were present at the experimental conditions. In most cases the analysis temperatures ($\sim T_h$) are significantly lower than those of entrapment. The fluid inclusions thus serve as solution cells for the spectroscopic study, as a function of temperature, of fluids equilibrated at known conditions. The fluid compositions are also idealized and quite different (especially R177) from what might be expected for natural ore-forming systems. Thus, this is not a study of analogs for natural fluids or even of fluids at the experimental entrapment conditions, but a spectroscopic study of defined fluids over an available temperature range. Nevertheless, this study has established the general importance of $[CuCl_2]^-$, the possible stability of $[CuCl_4]^{3-}$, and demonstrated how complex Cu *K*-absorption edges can be deconvoluted to allow the contributing species to be identified.

Finally, if higher-order Cu-Cl complexes are significant in natural brines, this may explain the partitioning behavior of Cu in porphyry/epithermal ore systems. From studies of coexisting vapor and brine phase inclusions, Cu has been found to partition into the vapor phase during boiling of a hydrothermal fluid (Heinrich et al. 1992, 1999). In the only case studied spectroscopically, $[CuCl_2]^-$ (or possibly $[CuCl(H_2O)]$) was identified as the complex present at T_h in the vapor phase inclusions (Mavrogenes et al. 2002). The partitioning of Cu as a Cl complex from a Cl-rich brine appears anomalous, but could derive from differences in the relative stability of the Cu^+ species. If higher order Cu complexes are electronically or energetically unstable relative to $[CuCl_2]^-$ (as indicated by their susceptibility to beam-induced decomposition), and if Cu is forced to occur as $[CuCl_{3/4}]^{2-/3-}$ in some natural ore-transporting brines due to the high concentration of Cl, then Cu may partition as $[CuCl_2]^-$ into the almost Cl^--free vapor phase produced during boiling as a means of reducing its coordination number. The increased stability of Cu as $[CuCl_2]^-$ in the Cl-poor

vapor compared to $[CuCl_{3/4}]^{2-/3-}$ in the Cl-rich brine may drive the partitioning. This speculative hypothesis suggests that boiling in a porphyry hydrothermal system, before the fixing of Cu as sulfides, may provide a mechanism for the transport of Cu from the porphyry environment to shallower levels, leading to the formation of Cu-bearing epithermal deposits.

ACKNOWLEDGMENTS

A.J.B., A.C.H., and J.A.M were supported at GSECARS by the Access to Major Research Facilities Program funded by the Commonwealth of Australia. A.C.H. thanks W.O. Hibberson, D.R. Scott, and S. O'Callaghan for assistance with sample preparation, C.G. Ryan for PIXE analyses, and the Australian National University for the award of a J.C. Jaeger Scholarship. We thank three anonymous reviewers whose comments significantly improved the manuscript. GeoSoilEnviroCARS is supported by the U.S. National Science Foundation (EAR-9906456) and the U.S. Department of Energy (DE-FG02-94ER14466). Use of the Advanced Photon Source was supported by the U.S. Department of Energy, Office of Science, Office of Basic Energy Sciences, under Contract No. W-31-109-Eng-38.

REFERENCES CITED

Akinfiev, N.N. and Zotov, A.V. (2001) Thermodynamic description of chloride, hydrosulfide, and hydroxo complexes of Ag(I), Cu(I), and Au(I) at temperatures of 25–500 °C and pressures of 1–2000 bar. Geochemistry International, 39, 990–1006.

Alcacio, T.E., Hesterberg, D., Chou, J.W., Martin, J.D., Beauchemin, S., and Sayers, D.E. (2001) Molecular scale characteristics of Cu(II) bonding in goethite-humite complexes. Geochimica et Cosmochimica Acta, 65, 1355–1366.

Anderson, A.J., Mayanovic, R.A., and Bajt, S. (1995) Determination of the local structure and speciation of zinc in individual hypersaline fluid inclusions by micro-xafs. Canadian Mineralogist, 33, 499.

Archibald, S.M., Migdisov, A.A., and Williams-Jones, A.E. (2002) An experimental study of the stability of copper chloride complexes in water vapor at elevated temperatures and pressures. Geochimica et Cosmochimica Acta, 66, 1611–1619.

Bair, R.A. and Goddard, W.A., III (1980) Ab initio studies of the X-ray absorption edge in copper complexes. I. Atomic Cu^{2+} and $Cu(II)Cl_2$. Physical Review B, 22, 2767–2776.

Bajt, S., Sutton, S.R., and Delaney, J.S. (1994) X-ray microprobe analysis of iron oxidation states in silicates and oxides using X-ray absorption near edge structure (XANES). Geochimica et Cosmochimica Acta, 58, 5209–5214.

Barnes, H.L. (1979) Geochemistry of Hydrothermal Ore Deposits, Second Edition, 798 p. Wiley-Interscience, New York.

Berry, A.J. and O'Neill, H.St.C. (2004) A XANES determination of the oxidation state of chromium in silicate glasses. American Mineralogist, 89, 790–798.

Berry, A.J., O'Neill, H.St.C., Jayasuriya, K.D., and Campbell, S.J. (2003) XANES calibrations for the oxidation state of iron in a silicate glass. American Mineralogist, 88, 967–977.

Blackburn, N.J., Strange, R.W., Reedijk, J., Volbeda, A., Farooq, A., Karlin, K.D., and Zubieta, J. (1989) X-ray absorption edge spectroscopy of copper(I) complexes. Coordination geometry of copper(I) in the reduced forms of copper proteins and their derivatives with carbon monoxide. Inorganic Chemistry, 28, 1349–1357.

Brodholt, J.P. and Wood, B.J. (1994) Measurements of the *PVT* properties of water to 25 kbars and 1600 °C. Geochimica et Cosmochimica Acta, 58, 2143–2148.

Collings, M.D., Sherman, D.M., and Ragnarsdottir, K.V. (2000) Complexation of Cu^{2+} in oxidized NaCl brines from 25 to 175 °C: results from in situ EXAFS spectroscopy. Chemical Geology, 167, 65–73.

Crerar, D.A. and Barnes, H.L. (1976) Ore solution chemistry. 5. Solubilities of chalcopyrite and chalcocite assemblages in hydrothermal solution at 200 to 350 °C. Economic Geology, 71, 772–794.

D'Angelo, P., Bottari, E., Festa, M.R., Nolting, H.-F., and Pavel, N.V. (1997) Structural investigation of copper(II) chloride solutions using X-ray absorption spectroscopy. Journal of Chemical Physics, 107, 2807–2812.

Eng, P.J., Newville, M., Rivers, M.L., and Sutton. S.R. (1998) Dynamically figured X-ray Kirkpatrick-Baez micro-focusing optics. SPIE Proceedings, 3449, 145–156.

Farges, F. (2005) Ab initio and experimental pre-edge investigations of the Mn *K*-edge XANES in oxide-type materials. Physical Review B, 71, 155109.

Fulton, J.L., Hoffmann, M.M., and Darab, J.G. (2000a) An X-ray absorption fine structure study of copper(I) chloride coordination structure in water up to 325 °C. Chemical Physics Letters, 330, 300–308.

Fulton, J.L., Hoffmann, M.M., Darab, J.G., Palmer, B.J., and Stern, E.A. (2000b) Copper(I) and copper(II) coordination structure under hydrothermal conditions at 325 °C: an X-ray absorption fine structure and molecular dynamics study. Journal of Physical Chemistry, 104, 11651–11663.

Garcia, J., Benfatto, M., Natoli, C.R., Bianconi, A., Fontaine, A., and Tolentino, H. (1989) The quantitative Jahn-Teller distortion of the Cu^{2+} site in aqueous solutions by XANES spectroscopy. Chemical Physics, 132, 295–307.

Giggenbach, W.F. (1987) Redox processes governing the chemistry of fumerolic gas discharges at White Island, New Zealand. Applied Geochemistry, 2, 143–161.

Günther, D., Audétat, A., Frischknecht, R., and Heinrich, C.A. (1998) Quantitative analysis of major, minor, and trace elements in fluid inclusions using laser ablation inductively coupled plasma mass spectrometry. Journal of Analytical Atomic Spectrometry, 13, 263–270.

Hack, A.C. and Mavrogenes, J.A. (2006) A synthetic fluid inclusion study of copper solubility in hydrothermal brines from 525 to 725 °C and 0.3 to 1.7 GPa. Geochimica et Cosmochimica Acta, in press.

Hamza, S., Khan, M.A., Lewonczuk, S., Ringeissen, J., Petiau, J., and Sainctavit, P. (1990) Conduction bands in CuCl and CuI by X-ray absorption at *K* and *L* edges. Solid State Communications, 75, 29–33.

Harris, A.C., Kamenetsky, V.S., White, N.C., van Achterbergh, E., and Ryan, C.G. (2003) Melt inclusions in veins: linking magmas and porphyry Cu deposits. Science, 302, 2109–2111.

Heinrich, C.A., Ryan C.G., Mernagh T.P., and Eadington P.J. (1992) Segregation of ore metals between magmatic brine and vapor—a fluid inclusion study using PIXE microanalysis. Economic Geology, 87, 1566–1583.

Heinrich, C.A., Günther, D., Audetat A., Ulrich, T., and Frischknecht, R. (1999) Metal fractionation between magmatic brine and vapor, determined by microanalysis of fluid inclusions. Geology, 27, 755–758.

Helz, G.R., Charnock, J.M., Vaughan, D.J., and Garner, C.D. (1993) Multinuclearity of aqueous copper and zinc bisulfide complexes: an EXAFS investigation. Geochimica et Cosmochimica Acta, 57, 15–25.

Hemley, J.J., Cygan, G.L., Fein, J.B., Robinson, G.R., and Dangelo, W.M. (1992) Hydrothermal ore-forming processes in the light of studies in rock-buffered systems. 1. Iron-copper-zinc-lead sulfide solubility relations. Economic Geology, 87, 1–22.

Hezarkhani, A., Williams-Jones, A.E., and Gammons, C.H. (1999) Factors controlling copper solubility and chalcopyrite deposition in the Sungun porphyry copper deposit, Iran. Mineralium Deposita, 34, 770–783.

Jayanetti, S., Mayanovic, R.A., Anderson, A.J., Bassett, W.A., and Chou, I.-M. (2001) Analysis of radiation-induced small Cu particle cluster formation in aqueous $CuCl_2$. Journal of Chemical Physics, 115, 954–962.

Kau, L.-S., Spira-Solomon, D.J., Penner-Hahn, J.E., Hodgson, K.O., and Solomon, E.I. (1987) X-ray absorption edge determination of the oxidation state and coordination number of copper: application to the type 3 site in Rhus vernicifera laccase and its reaction with oxygen. Journal of the American Chemical Society, 109, 6433–6442.

Liu, W.H., McPhail, D.C., and Brugger, J. (2001) An experimental study of copper(I)-chloride and copper(I)-acetate complexing in hydrothermal solutions between 50 and 250 °C and vapor-saturated pressure. Geochimica et Cosmochimica Acta, 65, 2937–2948.

Liu, W.H., Brugger, J., McPhail, D.C., and Spiccia, L. (2002) A spectrophotometric study of aqueous copper(I)-chloride complexes in LiCl solutions between 100 and 250 °C. Geochimica et Cosmochimica Acta, 66, 3615–3633.

Loucks, R.R. and Mavrogenes, J.A. (1999) Gold solubility in supercritical hydrothermal brines measured in synthetic fluid inclusions. Science, 284, 2159–2163.

Mavrogenes, J.A. and Bodnar, R.J. (1994) Hydrogen movement into and out of fluid inclusions in quartz: experimental evidence and geologic implications. Geochimica et Cosmochimica Acta, 58, 141–148.

Mavrogenes, J.A., Berry, A.J., Newville, M., and Sutton, S.R. (2002) Copper speciation in vapor-phase fluid inclusions from the Mole Granite, Australia. American Mineralogist, 87, 1360–1364.

Mountain, B.W. and Seward, T.M. (1999) The hydrosulphide/sulphide complexes of copper(I): experimental determination of stoichiometry and stability at 22 °C and reassessment of high temperature data. Geochimica et Cosmochimica Acta, 63, 11–29.

——— (2003) Hydrosulfide/sulfide complexes of copper(I): experimental confirmation of the stoichiometry and stability of $Cu(HS)_2^-$ to elevated temperatures. Geochimica et Cosmochimica Acta, 67, 3005–3014.

Onori, G., Santucci, A., Scafati, A., Belli, M., Della Longa, S., Bianconi, A., and Palladino, L. (1988) Cu *K*-edge XANES of Cu(II) ions in aqueous solution: a measure of the axial ligand distances. Chemical Physics Letters, 149, 289–294.

Palladino, L., Della Longa, S., Reale, A., Belli, M., Scafati, A., Onori, G., and Santucci, A. (1993) X-ray absorption near edge structure (XANES) of Cu(II)-ATP and related compounds in solution: quantitative determination of the distortion of the Cu site. Journal of Chemical Physics, 98, 2720–2726.

Romberger, S.B. and Barnes, H.L. (1970) Ore solution chemistry II. Solubility of CuS in sulfide solutions. Economic Geology, 65, 901–919.

Seward, T.M. and Barnes, H.L. (1997) Metal transport by hydrothermal ore fluids. In H.L. Barnes, Ed., Geochemistry of Hydrothermal Ore Deposits, Third Edition, p. 435–486. Wiley-Interscience, New York.

Seyfried, W.E. and Ding, K. (1993) The effect of redox on the relative solubilities

of copper and iron in Cl-bearing aqueous fluids at elevated temperatures and pressures—an experimental study with application to subseafloor hydrothermal systems. Geochimica et Cosmochimica Acta, 57, 1905–1917.
Shea, D. and Helz, G.R. (1988) The solubility of copper in sulfidic waters—sulfide and polysulfide complexes in equilibrium with covellite. Geochimica et Cosmochimica Acta, 52, 1815–1825.
Smith, T.A., Penner-Hahn, J.E., Berding, M.A., Doniach, S., and Hodgson, K.O. (1985) Polarized X-ray absorption edge spectroscopy of single-crystal copper(II) complexes. Journal of the American Chemical Society, 107, 5945–5955.
Sterner, S.M. and Bodnar, R.J. (1984) Synthetic fluid inclusions in natural quartz. I. Compositional types synthesized and applications to experimental geochemistry. Geochimica et Cosmochimica Acta, 48, 2659–2668.
Sutton, S.R., Jones, K.W., Gordon, B., Rivers, M.L., Bajt, S., and Smith, J.V. (1993) Reduced chromium in olivine grains from lunar basalt 15555: X-ray absorption near edge structure (XANES). Geochimica et Cosmochimica Acta, 57, 461–468.
Sverjensky, D.A., Shock, E.L., and Helgeson, H.C. (1997) Prediction of the thermodynamic properties of aqueous metal complexes to 1000 °C and 5 kb. Geochimica et Cosmochimica Acta, 61, 1359–1412.
Thompson, R.A. and Helz, G.R. (1994) Copper speciation in sulfidic solutions at low-sulfur activity—further evidence for cluster complexes. Geochimica et Cosmochimica Acta, 58, 2971–2983.
Varyash, L.N. (1991) Experimental study of Cu(I) complex formation in NaCl solutions at 300 and 350 °C. Geokhimiya, 1166–1174.
Varyash, L.N. and Rekharsky, V.I. (1981) Behavior of mono-valent copper in chloride solutions. Geokhimiya, 1003–1008.
Wong, J., Lytle, F.W., Messmer, R.P., and Maylotte, D.H. (1984) *K*-edge absorption spectra of selected vanadium compounds. Physical Review B, 30, 5596–5609.
Xiao, Z.F., Gammons, C.H., and Williams-Jones, A.E. (1998) Experimental study of copper(I) chloride complexing in hydrothermal solutions at 40 to 300 °C and saturated water vapor pressure. Geochimica et Cosmochimica Acta, 62, 2949–2964.

MANUSCRIPT RECEIVED MARCH 11, 2005
MANUSCRIPT ACCEPTED APRIL 28, 2006
MANUSCRIPT HANDLED BY JOHN AYERS